Intense chorus waves mitigate the loss of outer radiation belt relativistic electrons during storm main phase

S. Chakraborty[1], C.E.J. Watt[1], I.J. Rae[1], I.R. Mann[2], L. Olifer[2], A.W. Smith[1], J.-F. Ripoll[3,4], C.J. Rodger[5]

[1]Department of Mathematics, Physics and Electrical Engineering, Northumbria University, Newcastle upon Tyne, UK

[2]Department of Physics, University of Alberta, Edmonton, AB, Canada

[3]CEA, DAM, DIF, Arpajon, France

[4]UPS, CEA, LMCE, Bruyères-le-Châtel, France

[5]Department of Physics, University of Otago, Dunedin, New Zealand

Key Points:

- Intense chorus waves (power $> 10^{-4}$ nT^2) mitigate main phase loss of outer radiation belt ($L^* = 4 - 6$) relativistic electrons (E > 0.5 MeV)
- Loss mitigation from chorus waves is most effective at $L^* = 4.5$ in the energy range $1.1 - 2.6$ MeV during storm main phase ($-0.5 < $ t $ < 0$ day)
- Amount of lower energy (keV) electrons determines the consequences of the intense chorus waves on the relativistic electron population

Corresponding author: S. Chakraborty, `suman.chakraborty@northumbria.ac.uk`

Abstract

We investigate the effects of intense chorus waves (wave power $> 10^{-4}$ nT^2) on relativistic electrons (E > 0.5 MeV) in the heart of the outer radiation belt (L$^* = 4 - 6$) using superposed epoch approach. Combining electron flux and electromagnetic wave measurements from 70 geomagnetic storms during the Van Allen Probes mission, we show the relationship between integrated chorus wave power ($0.1 - 0.8$ equatorial electron gyrofrequency) and changes in relativistic electron flux on two hour timescales. During the loss-dominated storm main phase (Superposed Epoch -0.5 to 0 days), intense chorus waves mitigate the net loss of relativistic electrons. Conversely, in the early recovery phase (Superposed epoch 0 to 0.5 days), flux increases across a range of relativistic energies regardless of chorus wave power. The amount of electron flux at keV energies appears to have an influence on the consequences of chorus wave activity during geomagnetic storms.

Plain Language Summary

The Earth's radiation belt fluxes may vary by several orders of magnitude during periods of high geomagnetic activity. One of the candidates responsible for the rapid acceleration of electrons in the radiation belts is whistler-mode chorus waves. In this article, we investigate the effects of an intense population of the chorus waves on the relativistic electrons. Although the intense chorus waves are usually associated with energisation of the relativistic electrons, our results show that during geomagnetic storms they appear to mitigate loss processes that would otherwise occur in their absence. We also reveal the surprising result that when the radiation belts are enhanced in later times during geomagnetic storms, the amount of high energy electrons appears to increase regardless of whether the wave activity is high or low. We look at changes in the number of electrons at slightly lower energies and show that these electrons help to determine the consequences of intense chorus waves on the amount of high energy relativistic electrons. This new research provides critical insights into the chorus-driven wave-particle interactions that must be incorporated into models to study the complex dynamics of the radiation belts.

1 Introduction

Earth's outer radiation belt is a torus-shaped region filled with trapped charged particles between $\sim 2 - 7$ R$_E$. This is a highly dynamic region maintained by a competing balance between different acceleration, transport, and loss processes (Reeves et al., 2003; Baker et al., 2004; Summers et al., 2004; Hudson et al., 2008; J. Li et al., 2019; Ripoll et al., 2020; Lejosne et al., 2022). The study of this region is important to the space science community as our modern society has become increasingly reliant on space-based technologies. Sudden flux enhancements during geomagnetically active periods can damage electronic systems onboard satellites orbiting in this region of space which in some cases leads to total loss (Baker et al., 1997, 2018; Horne et al., 2013). The prediction of catastrophic events and the response of the radiation belts that lead to such events are therefore necessary to mitigate space weather hazards.

An immediate question that arises regarding the radiation belt variability is how intense the space radiation can get during periods of strong geomagnetic activity. In 1966, Kennel and Petschek suggested that there exists an upper limit to which the outer radiation belt electron fluxes can grow after which the fluxes get capped through the process of wave-particle interaction with whistler-mode waves (Kennel & Petschek, 1966). In the Kennel-Petschek (KP) paradigm, once the fluxes of the source population ($\sim 10 - 100$ keV) electrons reach close to or exceed a theoretical limit, whistler-mode wave growth becomes sufficiently strong. The waves then rapidly scatter electrons into the loss cone, thereby restricting the fluxes close to the theoretical limit. Recently, using 7 years of Van Allen Probe data, Olifer et al. (2021) and Chakraborty et al. (2022) provided direct ob-

servational evidence of this flux limitation process. Chakraborty et al. (2022) reported a distinct intense chorus wave population that is generated during the main phase of geomagnetic storms in the heart of the outer radiation belt. This intense wave population has wave power $2-3$ orders of magnitude larger than typical wave amplitudes and leads to the capping of the flux of tens of keV electrons. However, this study was limited to an examination of the ~10s of keV electrons which was not sufficient to provide a complete overview of the impact of the intense chorus waves on the outer radiation belt electron dynamics.

In this article, we study the effect of the short-lived intense chorus wave population on relativistic electrons (> 0.5 MeV). For this study, we use electron flux and electromagnetic wave measurements from the twin Van Allen Probes during 70 isolated geomagnetic storms spanning the Van Allen Probe era ($2012-2019$). By calculating the integrated wave power and fractional changes of electron fluxes in the energy range 0.75 -3.4 MeV, we statistically demonstrate the role of the intense chorus waves in the relativistic electron dynamics on two-hour timescales. Our results show that the waves that are generated to limit the flux of tens of keV electrons through the KP paradigm sequentially interact with higher energy electrons, and mitigate the loss processes effective in the outer radiation belt during the storm main phase (half a day before minimum Dst). During the early recovery phase (half a day after minimum Dst), the chorus waves are found to be less effective. In particular, flux increases after minimum Dst do not show a significant correlation with locally observed intense chorus wave power at least on two-hour timescales.

2 Data and Methodology

In this study, we examine trapped electron flux and electromagnetic wave measurements from the twin Van Allen Probes. We use the Level 3 pitch angle-resolved electron fluxes measured by the Magnetic Electron Ion Spectrometer (MagEIS) and Relativistic Electron-Proton Telescope (REPT), which are parts of the Energetic Particle, Composition, and Thermal Plasma (ECT) Suite (Baker et al., 2013; Blake et al., 2013; Spence et al., 2013). We consider 70 isolated geomagnetic storms during the entire Van Allen Probe era; the selection criteria and list can be found in Olifer et al. (2021) and Chakraborty et al. (2022). We take measurements from both Van Allen Probes and interpolate the measured flux with 2 hours of time resolution at specific L^* values. Next, we calculate the fractional flux change of electrons using the formula:

$$\Delta flux(t_i)\% = \frac{flux(t_i+1) - flux(t_i)}{flux(t_i)} \times 100\% \tag{1}$$

where flux(t_i) and flux(t_i+1) are the interpolated electron fluxes at two consecutive times. We calculate the electron fluxes and fractional change of electron fluxes for each storm event and then use superposed epoch analysis to determine the medians and interquartile ranges (IQRs). The storm epoch (T_0) is defined as the time of minimum Dst ($t = 0$) (Turner et al., 2019).

To calculate the integrated chorus wave power, we use wave magnetic field power spectral density (PSD) measurements from the Electric and Magnetic Field Instrument Suite and Integrated Science (EMFISIS) (Kletzing et al., 2013) with a time resolution of 6 seconds over 65 logarithmically spaced frequency bins from 1 Hz to 12 kHz. From the magnetic field PSD, chorus waves are identified using the following criteria as used in several studies (Bingham et al., 2018; Hartley et al., 2015, 2016, 2019, 2023; W. Li et al., 2014; Wang et al., 2019; Malaspina et al., 2020): (1) the PSD is $> 10^{-9}$ nT^2/Hz, (2) the waves are observed outside the plasmapause, defined here as density n_e below 30 #/cm^3 (see Ripoll et al. (2022)), and (3) the waves have planarity and ellipticity > 0.5 (Santolík et al., 2002, 2003). After identification of the chorus waves, the integrated wave power

117 (P_{ch}) is calculated within the frequency range $0.1 - 0.8$ f_{ce} (f_{ce} being the equatorial elec-
118 tron gyrofrequency). The temporal profile of integrated chorus wave power at specific
119 L^* is constructed for each storm event in a manner similar to the electron flux changes:
120 P_{ch} observations from both probes are interpolated with a 2-hour time resolution. When
121 no chorus waves are observed, P_{ch} is filled by 10^{-8} nT^2 representing an approximate noise
122 floor. Finally, superposed epoch analysis is performed to determine the medians and IQRs
123 of chorus wave power.

3 Results

125 Figure 1 demonstrates the statistical behavior of (a1) total and (a2) split chorus wave
126 power, (b1) background plasma electron number density, and (c1 – g1, c2 – g2) fractional
127 changes in electron flux across a range of energies ($0.75 - 3.4$ MeV). Panels (a1 – g1) in
128 the left column show the variations over a time span of ± 3 days, while panels (a2, c2
129 – g2) in the right column show the variations over a time span of ± 1 day relative to storm
130 epoch (T_0). The medians/IQRs of all observations in the analysis are shown using black
131 symbols. In the right-hand column, we split observations by chorus wave power and show
132 observations with intense chorus waves ($P_{ch} > 10^{-4}$ nT^2) in red symbols and observa-
133 tions with weaker chorus waves ($P_{ch} < 10^{-4}$ nT^2) in blue symbols. Figure 1 shows ob-
134 servations obtained for $4.45 < L^* < 4.55$ and $0 < MLT < 12$. The same analysis at L^*
135 $= 4 \pm 0.05$, 5 ± 0.05, and 5.5 ± 0.05 are provided in the supplementary material (Fig-
136 ures S1 – S3).

137 First, let us focus on the statistical results derived from all the events (Figure 1 panels
138 a1 – g1). The wave behavior for the three days before and after the storm (Figure 1 panel
139 a1) was originally demonstrated in Chakraborty et al. (2022) and displays dramatic en-
140 hancements above background levels starting from one day prior to T_0. The power then
141 peaks at $t = T_0$ and remains elevated above normal levels for at least one day after T_0.
142 The background electron number density (Figure 1 panel b1) is very variable across all
143 pre-storm phases but systematically decreases during the day before T_0. The median num-
144 ber density reaches a minimum of a tenth of pre-storm levels at T_0 where there is much
145 less variation between storms (i.e., a reduced IQR). The number density at $L^* = 4.5$ re-
146 mains depressed at $n_e \sim 10$ #/cc for ~ 2 days after the storm, recovering slowly toward
147 pre-storm levels.

148 For all energy channels from $0.75 - 3.4$ MeV (Figure 1 panels c1 – g1), during the pe-
149 riod $T_0 - 3 < t < T_0 - 0.5$ days, there is a pattern of very small fractional changes in
150 the flux and fractional increases are seen as often as fractional decreases (i.e., the me-
151 dian is near zero with small IQRs). During the period $T_0 - 0.5 < t < T_0$ days, there are
152 much larger changes, with more positive than negative changes in the lowest energy chan-
153 nel (panel c1), and more negative than positive changes in the higher energy channels
154 (panels e1 – g1). During the period $T_0 < t < T_0 + 1$ days, more positive fractional changes
155 are seen than negative changes across all energies (panels c1 – g1). After $T_0 + 1$ days,
156 across all energy channels, there are no large fractional changes in electron flux.

157 In the right-hand column of Figure 1 (panels c2 – g2), we present statistical results af-
158 ter splitting events by chorus wave power. The most significant differences in behavior
159 for different wave intensities occur in the period $T_0 - 0.5 < t < T_0$ days, although there
160 are some differences at other times. During the period $T_0 - 0.5 < t < T_0$ days, where
161 the chorus wave power is weak (blue symbols), the fractional changes in flux across all
162 energy channels are much more likely to be negative than positive. Where chorus wave
163 power is intense (red symbols), fractional changes in flux are more likely to be positive
164 than negative for low energies $0.75 - 1$ MeV (panels c2 and d2), or equally likely to be
165 positive or negative for higher energies $1.8 - 3.4$ MeV (panels e2 – g2). A similar pre-
166 sentation of observations at other L^* ranges (Figures S1 – S3) reveals similar behavior
167 to that seen in Figure 1, although the effect is most pronounced at $L^* = 4.5$.
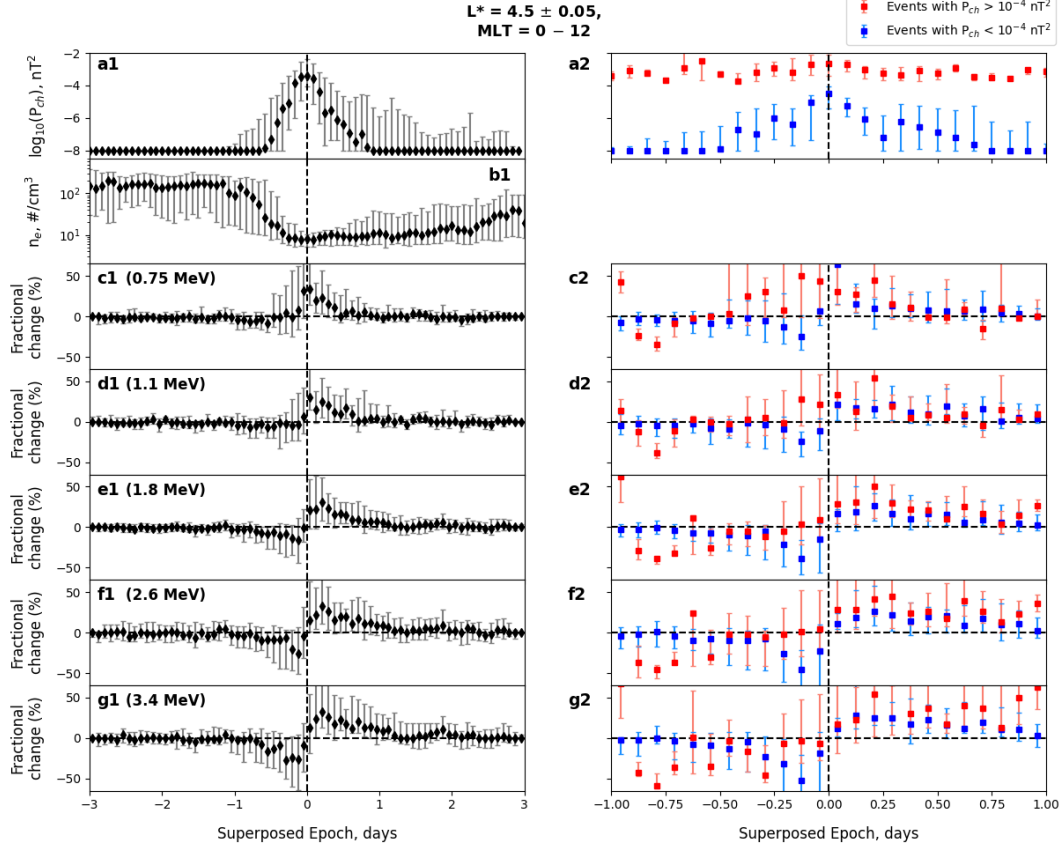
Figure 1. Superposed epoch analysis of (a1) integrated chorus wave power $(0.1 - 0.8\ f_{ce})$, (b1) background plasma electron number density n_e $(\#/cm^3)$, and fractional change of trapped electron fluxes of (c1) 0.75 MeV and (d1) 1.1 MeV electrons from the MagEIS instrument, and (e1) 1.8 MeV, (f1) 2.6 MeV and (g1) 3.4 MeV electrons from the REPT instrument at $L^* = 4.5 \pm 0.05$ and $0 - 12$ MLT during ± 3 days around epoch day 0. Panels (a2) and (c2 – g2) show corresponding variations in the integrated chorus wave power and fractional changes in electron fluxes during ± 1 day around epoch day 0 splitting the total power in two ranges. The red data points correspond to events during which the integrated chorus wave power exceeded 10^{-4} nT^2, while the blue data points correspond to events during which the integrated chorus wave power remained low and did not exceed 10^{-4} nT^2. In each panel, the median and interquartile ranges are plotted as a function of superposed epoch days. The vertical dashed line in each panel denotes storm time epoch which corresponds to the time of storm maximum (minimum SYM-H).

Changes in flux during the period immediately prior to T_0 appear to be ordered by wave power on two-hour timescales, motivating us to study this parameter in more detail. Figure 2 specifically relates the strength of the chorus waves directly to fractional changes in electron flux at each energy during four phases of geomagnetic storms defined as (i) pre-storm phase: $T_0 - 3 < t < T_0 - 0.5$ days (column 1); (ii) main phase: $T_0 - 0.5 < t < T_0$ days (column 2); (iii) early recovery phase: $T_0 < t < T_0 + 0.5$ days (column 3); and (iv) late recovery phase: $T_0 + 0.5 < t < T_0 + 3$ days (column 4). Here, the storm phases are defined based on the wave activity, viz., the main and early recovery phases encompass periods during which the integrated chorus wave power tends to be high, and the pre-storm and late recovery phases encompass periods during which the integrated chorus power tends to be low. As in Figure 1, the data shown in Figure 2 are for 4.45 $< L^* < 4.55$ and $0 < MLT < 12$. The same analysis at other L^* values are provided in the supplementary material (Figures S4 – S6). In all of these figures, the top row indicates the number of observations in each wave power bin with a bin width of 0.5 in the base-10 log of the wave power. The following five rows show the medians and IQRs of fractional flux changes in each energy channel corresponding to each wave power bin. The colorbar at the right denotes the median fractional flux changes, where red indicates an increase in the flux, white indicates no/small flux changes, and blue indicates a decrease in the flux.

In the pre-storm phase (column 1), the electron fluxes do not vary significantly when the wave power is low, i.e., the medians of fractional changes in electron fluxes stay close to zero with small IQRs. As wave power increases, flux variations are still mostly balanced around zero (the horizontal dotted line) for low energies (panels e and i), whereas at the higher energies (panels m, q, and u), the medians exhibit negative values ($\sim$ –20 to $\sim$ –30%) for higher wave power indicating decreases in trapped fluxes. The occurrence distribution of waves (panel a) shows that there is a very low occurrence of high-power waves during this period, but those that do exist are associated with trapped flux decreases for $1.8 \leq E \leq 3.4$ MeV.

In the main phase (column 2), when wave power is low, the medians of fractional change of fluxes at all energies exhibit negative values denoting decreases in fluxes, with greater decreases ($\sim$ –50%) at higher energies. As wave power increases, the medians of fractional changes gradually shift to higher values. Electrons with energies in the range 1.1 – 2.6 MeV (panels j, n, r) show a systematic variation in fractional changes with wave power. At these energies, as wave power increases, the medians of the fractional changes exhibit a progressive increase toward positive/zero values. At lower and higher energies, the correlation is weaker (panels f and v). The occurrence distribution of wave power (panel b) during this period further shows a high occurrence rate of high power waves, centered around $\sim 10^{-4}$ nT^2. Therefore, the results suggest that the presence of high-power chorus waves during the main phase of geomagnetic storms which is otherwise loss-dominated at relativistic energies leads to a reduction in the level of loss across this energy range.

In the early recovery phase (column 3), the medians and lower quartiles of fractional flux changes exhibit positive values denoting increment in fluxes. Possible losses are not only mitigated as in the main phase, there now is a supply of electrons, possibly from chorus acceleration. We see continuity from the main to early recovery phases, with a gradual change from negative to positive fractional flux changes. The correlation with integrated chorus wave power is not as strong as in the main phase, though waves with P_{ch} $> 10^{-4}$ nT^2 are associated with slightly larger fractional increases in flux at all energies.

In the late recovery phase (column 4), fluxes don't show any significant variations with the chorus wave power, i.e., the medians of fractional flux changes stay close to zero with small IQRs for $E = 0.75$ and 1.1 MeV. Only at the higher energies (panels p, t and x) do we see a change in the medians of the fractional flux changes with chorus wave power.
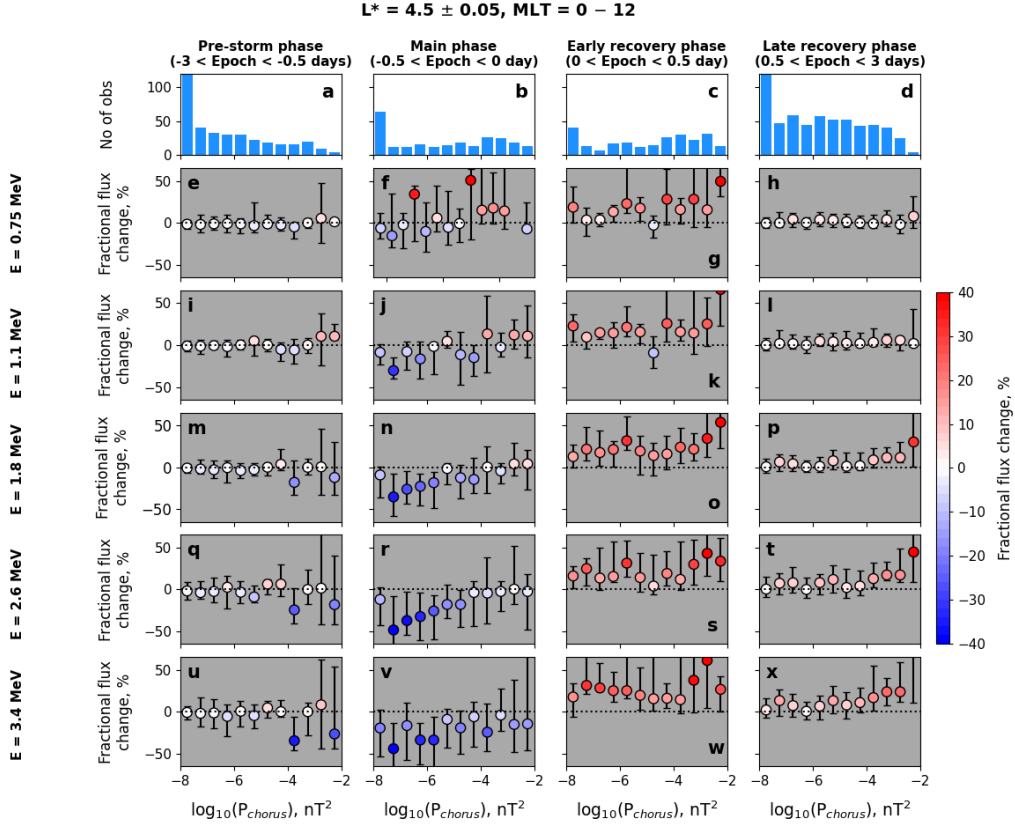
Figure 2. Correlation between integrated chorus wave power and fractional change of electron fluxes during four phases of geomagnetic storms: pre-storm phase ($-3 <$ Epoch day < -0.5), main phase ($-0.5 <$ Epoch day < 0), early recovery phase ($-0 <$ Epoch day < 0.5), and late recovery phase ($0.5 <$ Epoch day < 3) at $L^* = 4.5 \pm 0.05$ and $0 - 12$ MLT. Panels (a – d) show the number of observations in each wave power bin during the four storm phases. Panels (e – x) show the medians and interquartile ranges. The colorbar at the right denotes the fractional changes in electron fluxes, where red indicates a positive change, white indicates no/a small change, and blue indicates a negative change.

Where wave power is intense ($P_{ch} > 10^{-4}$ nT^2), there are significant positive changes with wave power.

A similar analysis at other L^* ranges (Figures S4 – S6) reveals similar behavior, although the effect is most pronounced at $L^* = 4.5$, reconfirming the findings from Figure 1. Figure 2 demonstrates new interesting relationships: (i) in the pre-storm phase, at energies ≥ 1.8 MeV, there is a weak relationship between higher chorus wave power and negative fractional flux changes, (ii) in the storm main phase, and especially for $1.1 \leq E \leq 2.6$ MeV, there is a strong indication that increasing chorus wave power mitigates the large flux decreases that would otherwise occur in the absence of high chorus wave power, (iii) in the early recovery phase, fractional increases in flux occur across all energies with no strong dependence on the chorus wave power and (iv) in the late recovery phase, for $1.8 \leq E \leq 3.4$ MeV, there is a relationship between chorus wave power and fractional increases in flux, especially for higher values of chorus wave power.

4 Discussion

Previously, Chakraborty et al. (2022) demonstrated that intense chorus waves occur during the main phase and early recovery phase of the storm only once the electron flux of tens to hundreds of keV electrons reach or exceeds the threshold identified by Kennel and Petschek (1966). In this paper, we demonstrate that intense chorus waves seen during geomagnetic storms are important not only for their role in limiting the flux of tens to hundreds of keV electrons but also for changing the response of the trapped relativistic electrons during the storm.

The strongest effect seen in the statistical analysis of the observations is that during the main phase of the storm ($T_0 - 0.5 < t < T_0$ days) the presence of intense chorus waves mitigates the reduction in trapped electron fluxes across a range of different energies ($0.75 \leq E \leq 2.6$ MeV) in the outer radiation belt ($4 < L^* < 6$). Strong reductions in flux in the main phase occur when intense chorus waves are absent (see second column of Figure 2). However, during this phase, if intense chorus waves are present, they result in significantly smaller decreases in flux, or even small increases in flux, over shorter two-hour periods. Note that the power of chorus waves during this storm phase is highly variable (see the variability in Figure 1 panel 1a, and the histogram in Figure 2b), and so the overall outcome of the storm main phase remains electron dropout (e.g. Morley et al. (2010); Turner et al. (2014); Murphy et al. (2018)). The depth in flux of the dropout may be controlled by the presence or lack of intense chorus waves.

Conversely, periods of enhancements in relativistic electron flux in the early recovery phase, which are accompanied by intense chorus waves (see Figure 1 panel a1), do not appear to have a strong relationship with chorus wave power. In particular, we see positive fractional flux changes occurring at very low chorus power. We must therefore conclude that other processes have a stronger influence on radiation belt enhancements during the early recovery phase of storms. For example, the statistical analysis of Murphy et al. (2018) indicates that radial diffusion may be related to increases in flux in storm recovery phases because of a strong association with the amplitude of ULF waves in the magnetosphere. Our results demonstrate the lack of a strong or obvious contribution by intense chorus waves during early recovery phase, even though chorus waves are likely to be seen during this period (see Figure 1 panel a1).

In the discussion to follow, we will consider increases and decreases in electron flux over a wider range of energies in order to explain our findings, in addition to three essential criteria required for chorus-driven acceleration to be effective:

1. Abundance of the source electron population (tens of keV) that generates the chorus waves and seed electron population (hundreds of keV) that are in turn accelerated by the chorus waves to relativistic energies. The absence of any of these elements in the radiation belts ceases the acceleration process (Jaynes et al., 2015).
2. Abundance of high wave power, which Chakraborty et al. (2022) demonstrates is a result of low-energy fluxes (item 1 above) exceeding the threshold identified by Kennel and Petschek (1966).
3. A low background plasma density that creates a preferential condition for the local diffusive acceleration of electrons from hundreds of keV to several MeV (Allison et al., 2021).

Figure 3 summarizes the three essential criteria described above for effective chorus-driven acceleration. Panels (a – d) show the superposed epoch analyses of fractional flux changes at energies spanning the source, seed, and relativistic electron populations (30 keV – 4.5 MeV) at four specific L^* ranges. The colorbar at the right indicates the median values of fractional flux changes in each energy bin, where red indicates a positive change (acceleration/energization), blue indicates a negative change (loss), and white indicates no/small

change in trapped fluxes. Contour lines for 20% and 40% increase/decrease in flux are shown with solid black lines to highlight periods of significant flux variations. There are four important points to note from panels (a – d): (i) At all L^* ranges, the significant flux variations (increase/decrease) happen mostly within epoch day ± 0.5, with a noticeable time delay from the lowest to the highest energies. This indicates that increases in electron flux in a particular energy bin occur only when electron flux in a lower energy bin has also started increasing. (ii) The source electron population exhibits an initial strong acceleration followed by a loss, and the seed electron population exhibits a strong acceleration followed by no/small flux variations. For the relativistic electron population, sub-MeV electron fluxes exhibit an increase followed by a gradual decrease to the pre-storm flux levels. The long duration of this loss (gradual negative fractional flux from 100 to 800 keV) and the fact that it is more statistically visible at low L^* than at higher L^* (i.e., more in the plasmasphere) concur to suggest that this loss is whistler-mode hiss driven following the recovering and expanding plasmasphere after the storm (Ripoll et al., 2019; Pierrard et al., 2021). Above 1 MeV electron fluxes exhibit an initial loss followed by strong acceleration. (iii) The switch from loss to acceleration of > MeV electrons happens at epoch day 0 at all L^* ranges when the chorus waves are at their peak. (iv) A complete sequential strong acceleration from the lowest to the highest energies happens only at $L^* = 4.5$. (c.f. Figure 3 in Murphy et al. (2018) which shows a similar pattern in a different coordinate system that lacks distinction in L^*).

The above points considered alongside criterion (1) suggest why intense chorus wave-driven acceleration is effective during the storm main phase ($T_0 - 0.5 < t < T_0$ days), but not effective during the early recovery phase ($T_0 < t < T_0 + 0.5$ days). During the main phase, fluxes of the source electron population (tens of keV) increase significantly which can be attributed to fresh injection of electrons at these energies by storm-triggered sub-storm activities. As the fluxes of these electrons increase and exceed the Kennel-Petschek threshold, intense chorus waves are generated and scatter the electrons into the loss cone to deplete the excess electrons and maintain the fluxes close to the threshold (Chakraborty et al., 2022). This marks the loss phase of the source electron population in the early recovery phase. For the seed population (100s of keV), fluxes never cross the Kennel-Petschek threshold. Instead, fluxes are typically saturated at the threshold (Olifer et al., 2021), which marks the no/small flux variation phase after T_0. Looking now at MeV energies, the main phase ($T_0 - 0.5 < t < T_0$ days) is marked by significant reductions in flux that appear to be independent of the acceleration at lower energies. As demonstrated in Figure 2, the intense chorus waves generated when the source population exceeds the Kennel-Petschek threshold act to mitigate this independent loss process. During the recovery phase ($T_0 < t < T_0 + 0.5$ days), although there are intense chorus waves, the seed population is decreasing or constant, thus removing an important criterion for chorus-driven acceleration to continue to higher energies.

Throughout the study, we see that effects are most pronounced at $L^* = 4.5$. To demonstrate why this is the case, panels (e) and (f) of Figure 3 show the radial profiles (medians and IQRs) of integrated chorus wave power and background plasma density at three specific epochs: epoch day – 0.5 (blue), epoch day 0 (black), and epoch day 0.5 (red). In panels (a – d), the three vertical dashed lines correspond to the specific epochs at which the radial profiles are plotted. Panel (e) shows that the radial profile of integrated chorus wave power at epoch days –0.5 (blue) and 0.5 (red) exhibit a monotonic increase towards larger L^* values, indicating that higher power waves exist at outer radial distances during these epochs. On the contrary, at epoch day 0 (black), the radial profile is found to peak at $L^* = 4.5$. In addition, at this epoch, the wave power is $\sim 2 - 3$ orders of magnitude higher than those during the other two epochs at almost all the L^* ranges. In the supporting document, we have provided a movie showing the evolution of the radial profile of the integrated chorus wave power during the period $T_0 - 0.5 < t < T_0 + 0.5$. The movie clearly shows the peak of the wave power to shift towards $L^* = 4.5$ during $T_0 - 0.5 < t < T_0$ days, and then return back to pre-storm profiles during $T_0 < t < T_0 +$
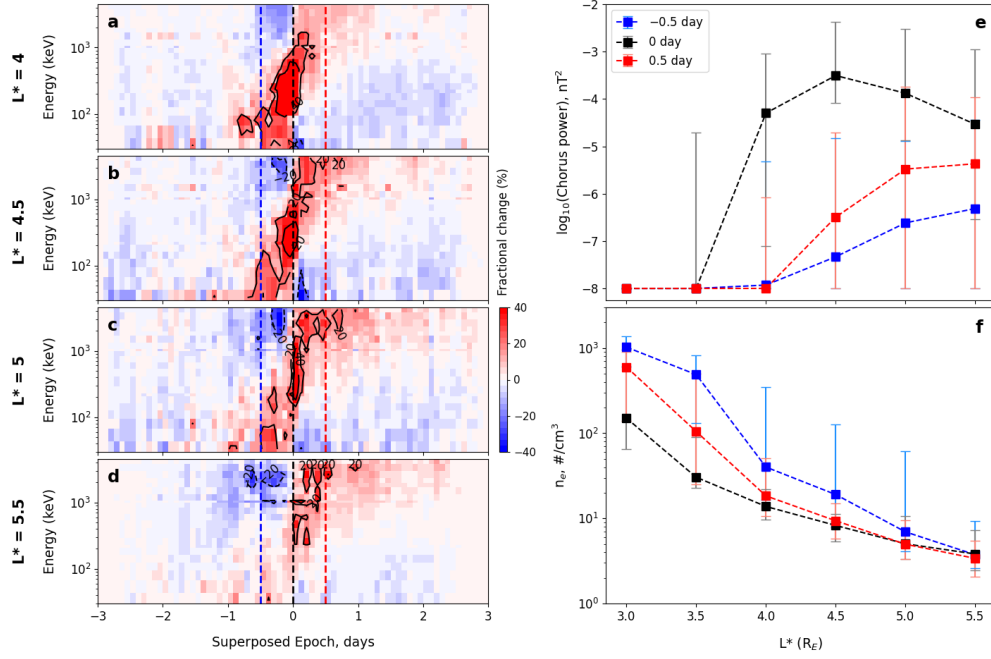
Figure 3. Superposed epoch analyses of fractional change of fluxes of electrons in the energy range 30 keV to 4.2 MeV at (a) $L^* = 4$, (b) $L^* = 4.5$, (c) $L^* = 5$, and (d) $L^* = 5.5$. The colorbar at the right denotes the median value of fraction flux changes in each energy bin, where red indicates a positive change (increase/acceleration), blue indicates a negative change (decrease/loss), and white indicates no/small change in flux. Contour lines for 20% and 40% increase/decrease in flux are included in panels (a – d) to highlight periods of significant flux changes. The three dashed vertical lines in panels (a – d) indicate the times at which radial profiles of integrated chorus wave power (nT^2) in logarithmic scale and background plasma density n_e ($\#/cm^3$) are plotted in panels (e) and (f) respectively. Medians and interquartile ranges of wave power and plasma density are plotted as a function of L^* at three epoch days within the storm main phase: epoch day -0.5 (blue), epoch day 0 (black), and epoch day 0.5 (red).

0.5 days. The background plasma density is also found to be significantly lower during epoch day 0 (median of $n_e \approx 10/cm^3$) at $L^* = 4.5$ (panel f), compared to lower L^* ranges, while at higher L^* ranges, the difference between the background plasma density at different epochs is negligible. Thus, combining results from panels (e) and (f) and criteria (2) and (3), we found that the integrated chorus wave power increases by $2 - 3$ orders of magnitude at epoch day 0 peaking at $L^* = 4.5$. In addition, the plasma density at this epoch at $L^* = 4.5$ is also considerably low, thereby favoring the chorus-driven acceleration to be effective, thus corroborating the findings from Figures 1 and 2.

These results demonstrate that there are a number of key physical factors that should be included in radiation belt models in order to reproduce the effects of intense chorus waves during geomagnetic storms, both to capture their effects on relativistic electrons in the main phase, and also to prevent the observed intense chorus waves resulting in too much energisation during the early recovery phase:

1. Intense chorus waves are rare in the Van Allen Probe record, and models of wave activity should be built using algorithms that accommodate the uneven sampling of rare large values (e.g. Chu et al. (2023)). Models could be parameterised by the proximity of 10-100s keV flux to the Kennel-Petschek threshold.
2. The electron density that feeds into diffusion coefficient models should include the reduction in number density observed in storms (see e.g. Fig 2, Watt et al. (2021)).
3. Energy-boundary flux models must incorporate appropriate limiting or reduction in the seed population flux in the early recovery phase to ensure that a realistic model of the chorus wave amplitudes during storms (see point 1) does not result in too much enhancement of flux at relativistic energies.

5 Conclusion

In this study, we demonstrate the effects of intense large-amplitude whistler-mode chorus waves on the relativistic electrons in the heart of the outer radiation belt. Using a statistical analysis of 70 geomagnetic storms, we specifically study the fractional increases and decreases of relativistic electron flux and compare these to the strength of the chorus waves during different phases of storms. Our results show that intense chorus waves, which have wave powers $\sim 2 - 3$ orders of magnitude larger than the ambient waves, affect electrons predominantly in the main phase and particularly in the energy range 1.1 $- 2.6$ MeV in the outer radiation belt ($L^* = 4 - 5.5$). The acceleration resulting from chorus wave-particle interaction balances out significant decreases in relativistic electron flux during the storm main phase that otherwise occurs when the intense chorus waves are absent. Intriguingly, during the early recovery phase where intense chorus waves are equally likely to exist, enhancements in relativistic electron flux appear to be not strongly dependent on the strength of the chorus. During the early recovery phase, when the 10 $- 100$ keV seed population is limited by the effects predicted by Kennel and Petschek (1966), further acceleration by the intense chorus waves gets limited. Enhancements in relativistic electron flux during the early recovery phase must therefore be attributed to other radiation belt processes.

6 Open Research

References

Allison, H. J., Shprits, Y. Y., Zhelavskaya, I. S., Wang, D., & Smirnov, A. G. (2021). Gyroresonant wave-particle interactions with chorus waves during extreme depletions of plasma density in the Van Allen radiation belts. *Science Advances*, *7*(5). doi: 10.1126/sciadv.abc0380

Baker, D. N., Erickson, P. J., Fennell, J. F., Foster, J. C., Jaynes, A. N., & Verronen, P. T. (2018). Space Weather Effects in the Earth's Radiation Belts. *Space Science Reviews*, *214*(1). doi: 10.1007/s11214-017-0452-7

Baker, D. N., Kanekal, S. G., & Blake, J. B. (2004). Characterizing the Earth's outer Van Allen zone using a radiation belt content index. *Space Weather*, *2*(2). doi: 10.1029/2003SW000026

Baker, D. N., Kanekal, S. G., Hoxie, V. C., Batiste, S., Bolton, M., Li, X., . . . Friedel, R. (2013). The Relativistic Electron-Proton Telescope (REPT) Instrument on Board the Radiation Belt Storm Probes (RBSP) Spacecraft: Characterization of Earthâ€™s Radiation Belt High-Energy Particle Populations. *Space Science Review*, *179*(1). doi: 10.1007/s11214-012-9950-9

Baker, D. N., Li, X., Turner, N., Allen, J. H., Bargatze, L. F., Blake, J. B., . . . Rostoker, G. (1997). Recurrent geomagnetic storms and relativistic electron enhancements in the outer magnetosphere: ISTP coordinated measurements. *Journal of Geophysical Research: Space Physics*, *102*(A7), 14141-14148. doi: 10.1029/97JA00565

Bingham, S. T., Mouikis, C. G., Kistler, L. M., Boyd, A. J., Paulson, K., Farrugia, C. J., . . . Kletzing, C. (2018). The Outer Radiation Belt Response to the Storm Time Development of Seed Electrons and Chorus Wave Activity During CME and CIR Driven Storms. *Journal of Geophysical Research: Space Physics*, *123*(12), 10,139-10,157. doi: 10.1029/2018JA025963

Blake, J. B., Carranza, P. A., Claudepierre, S. G., Clemmons, J. H., Crain Jr., W. R., Dotan, Y., . . . Zakrzewski, M. P. (2013). The Magnetic Electron Ion Spectrometer (MagEIS) Instruments Aboard the Radiation Belt Storm Probes (RBSP) Spacecraft. *Space Science Review*, *179*, 383–421. doi: 10.1007/s11214-013-9991-8

Chakraborty, S., Mann, I. R., Watt, C. E. J., Rae, I. J., Olifer, L., Ozeke, L. G., . . . Spence, H. (2022). Intense chorus waves are the cause of flux-limiting in the heart of the outer radiation belt. *Scientific Reports*, *12*(1). doi: 10.1038/s41598-022-26189-9

Chu, X., Bortnik, J., Li, W., Shen, X.-C., Ma, Q., Ma, D., . . . Huang, S. (2023). Distribution and Evolution of Chorus Waves Modeled by a Neural Network: The Importance of Imbalanced Regression. *Space Weather*, *21*(10). doi: 10.1029/2023SW003524

Hartley, D. P., Chen, Y., Kletzing, C. A., Denton, M. H., & Kurth, W. S. (2015). Applying the cold plasma dispersion relation to whistler mode chorus waves: EMFISIS wave measurements from the Van Allen Probes. *Journal of Geophysical Research: Space Physics*, *120*(2), 1144-1152. doi: 10.1002/2014JA020808

Hartley, D. P., Christopher, I. W., Kletzing, C. A., Kurth, W. S., Santolik, O.,

Kolmasova, I., ... Ahmadi, N. (2023). Chorus Wave Properties From Van Allen Probes: Quantifying the Impact of the Sheath Corrected Electric Field. *Geophysical Research Letters*, *50*(7), e2023GL102922. doi: 10.1029/2023GL102922

Hartley, D. P., Kletzing, C. A., Chen, L., Horne, R. B., & Santolík, O. (2019). Van Allen Probes Observations of Chorus Wave Vector Orientations: Implications for the Chorus-to-Hiss Mechanism. *Geophysical Research Letters*, *46*(5), 2337-2346. doi: 10.1029/2019GL082111

Hartley, D. P., Kletzing, C. A., Kurth, W. S., Bounds, S. R., Averkamp, T. F., Hospodarsky, G. B., ... Watt, C. E. J. (2016). Using the cold plasma dispersion relation and whistler mode waves to quantify the antenna sheath impedance of the Van Allen Probes EFW instrument. *Journal of Geophysical Research: Space Physics*, *121*(5), 4590-4606. doi: 10.1002/2016JA022501

Horne, R. B., Glauert, S. A., Meredith, N. P., Boscher, D., Maget, V., Heynderickx, D., & Pitchford, D. (2013). Space weather impacts on satellites and forecasting the Earth's electron radiation belts with SPACECAST. *Space Weather*, *11*(4), 169-186. doi: 10.1002/swe.20023

Hudson, M. K., Kress, B. T., Mueller, H.-R., Zastrow, J. A., & Bernard Blake, J. (2008). Relationship of the Van Allen radiation belts to solar wind drivers. *Journal of Atmospheric and Solar-Terrestrial Physics*, *70*(5), 708-729. doi: 10.1016/j.jastp.2007.11.003

Jaynes, A. N., Baker, D. N., Singer, H. J., Rodriguez, J. V., Loto'aniu, T. M., Ali, A. F., ... Reeves, G. D. (2015). Source and seed populations for relativistic electrons: Their roles in radiation belt changes. *Journal of Geophysical Research: Space Physics*, *120*(9), 7240-7254. doi: 10.1002/2015JA021234

Kennel, C. F., & Petschek, H. E. (1966). Limit on stably trapped particle fluxes. *Journal of Geophysical Research (1896-1977)*, *71*(1), 1-28. doi: 10.1029/JZ071i001p00001

Kletzing, C. A., Kurth, W. S., Acuna, M., MacDowall, R. J., Torbert, R. B., Averkamp, T., ... Tyler, J. (2013). The Electric and Magnetic Field Instrument Suite and Integrated Science (EMFISIS) on RBSP. *Space Science Review*, *179*, 127–181. doi: 10.1007/s11214-013-9993-6

Lejosne, S., Allison, H. J., Blum, L. W., Drozdov, A. Y., Hartinger, M. D., Hudson, M. K., ... Zhao, H. (2022). Differentiating Between the Leading Processes for Electron Radiation Belt Acceleration. *Frontiers in Astronomy and Space Sciences*, *9*. doi: 10.3389/fspas.2022.896245

Li, J., Bortnik, J., An, X., Li, W., Angelopoulos, V., Thorne, R. M., ... Baker, D. N. (2019). Origin of two-band chorus in the radiation belt of Earth. *Nature Communications*, *10*(1). doi: 10.1038/s41467-019-12561-3

Li, W., Mourenas, D., Artemyev, A. V., Agapitov, O. V., Bortnik, J., Albert, J. M., ... Hospodarsky, G. B. (2014). Evidence of stronger pitch angle scattering loss caused by oblique whistler-mode waves as compared with quasi-parallel waves. *Geophysical Research Letters*, *41*(17), 6063-6070. doi: 10.1002/2014GL061260

Malaspina, D. M., Zhu, H., & Drozdov, A. Y. (2020). A Wave Model and Diffusion Coefficients for Plasmaspheric Hiss Parameterized by Plasmapause Location. *Journal of Geophysical Research: Space Physics*, *125*(2), e2019JA027415. doi: 10.1029/2019JA027415

Morley, S. K., Friedel, R. H. W., Spanswick, E. L., Reeves, G. D., Steinberg, J. T., Koller, J., ... Noveroske, E. (2010). Dropouts of the outer electron radiation belt in response to solar wind stream interfaces: global positioning system observations. *Proceedings of the Royal Society A: Mathematical, Physical and Engineering Sciences*, *466*(2123), 3329-3350. doi: 10.1098/rspa.2010.0078

Murphy, K. R., Watt, C. E. J., Mann, I. R., Jonathan Rae, I., Sibeck, D. G., Boyd, A. J., ... Fennell, J. (2018). The Global Statistical Response of the Outer Radiation Belt During Geomagnetic Storms. *Geophysical Research Letters*,

45(9), 3783-3792. doi: 10.1002/2017GL076674

Olifer, L., Mann, I. R., Kale, A., Mauk, B. H., Claudepierre, S. G., Baker, D. N., . . . Ozeke, L. G. (2021). A Tale of Two Radiation Belts: The Energy-Dependence of Self-Limiting Electron Space Radiation. *Geophysical Research Letters*, *48*(20). doi: 10.1029/2021GL095779

Pierrard, V., Ripoll, J.-F., Cunningham, G., Botek, E., Santolik, O., Thaller, S., . . . Cosmides, M. (2021). Observations and Simulations of Dropout Events and Flux Decays in October 2013: Comparing MEO Equatorial With LEO Polar Orbit. *Journal of Geophysical Research: Space Physics*, *126*(6). doi: 10.1029/2020JA028850

Reeves, G. D., McAdams, K. L., Friedel, R. H. W., & O'Brien, T. P. (2003). Acceleration and loss of relativistic electrons during geomagnetic storms. *Geophysical Research Letters*, *30*(10). doi: 10.1029/2002GL016513

Ripoll, J.-F., Claudepierre, S. G., Ukhorskiy, A. Y., Colpitts, C., Li, X., Fennell, J. F., & Crabtree, C. (2020). Particle Dynamics in the Earth's Radiation Belts: Review of Current Research and Open Questions. *Journal of Geophysical Research: Space Physics*, *125*(5), e2019JA026735. doi: 10.1029/2019JA026735

Ripoll, J.-F., Loridan, V., Denton, M. H., Cunningham, G., Reeves, G., Santolík, O., . . . Ukhorskiy, A. Y. (2019). Observations and Fokker-Planck Simulations of the L-Shell, Energy, and Pitch Angle Structure of Earth's Electron Radiation Belts During Quiet Times. *Journal of Geophysical Research: Space Physics*, *124*(2), 1125-1142. doi: 10.1029/2018JA026111

Ripoll, J.-F., Thaller, S. A., Hartley, D. P., Cunningham, G. S., Pierrard, V., Kurth, W. S., . . . Wygant, J. R. (2022). Statistics and Empirical Models of the Plasmasphere Boundaries From the Van Allen Probes for Radiation Belt Physics. *Geophysical Research Letters*, *49*(21), e2022GL101402. doi: 10.1029/2022GL101402

Santolík, O., Parrot, M., & Lefeuvre, F. (2003). Singular value decomposition methods for wave propagation analysis. *Radio Science*, *38*(1). doi: 10.1029/2000RS002523

Santolík, O., Pickett, J. S., Gurnett, D. A., & Storey, L. R. O. (2002). Magnetic component of narrowband ion cyclotron waves in the auroral zone. *Journal of Geophysical Research: Space Physics*, *107*(A12), SMP 17-1-SMP 17-14. doi: 10.1029/2001JA000146

Spence, H. E., Reeves, G. D., Baker, D. N., Blake, J. B., Bolton, M., Bourdarie, S., . . . Thorne, R. M. (2013). Science Goals and Overview of the Radiation Belt Storm Probes (RBSP) Energetic Particle, Composition, and Thermal Plasma (ECT) Suite on NASA's Van Allen Probes Mission. *Space Science Review*, *179*, 311–336. doi: 10.1007/s11214-013-0007-5

Summers, D., Ma, C., & Mukai, T. (2004). Competition between acceleration and loss mechanisms of relativistic electrons during geomagnetic storms. *Journal of Geophysical Research: Space Physics*, *109*(A4). doi: 10.1029/2004JA010437

Turner, D. L., Angelopoulos, V., Morley, S. K., Henderson, M. G., Reeves, G. D., Li, W., . . . Rodriguez, J. V. (2014). On the cause and extent of outer radiation belt losses during the 30 September 2012 dropout event. *Journal of Geophysical Research: Space Physics*, *119*(3), 1530-1540. doi: 10.1002/2013JA019446

Turner, D. L., Kilpua, E. K. J., Hietala, H., Claudepierre, S. G., O'Brien, T. P., Fennell, J. F., . . . Reeves, G. D. (2019). The Response of Earth's Electron Radiation Belts to Geomagnetic Storms: Statistics From the Van Allen Probes Era Including Effects From Different Storm Drivers. *Journal of Geophysical Research: Space Physics*, *124*(2), 1013-1034. doi: 10.1029/2018JA026066

Wang, D., Shprits, Y. Y., Zhelavskaya, I. S., Agapitov, O. V., Drozdov, A. Y., & Aseev, N. A. (2019). Analytical Chorus Wave Model Derived from Van Allen Probe Observations. *Journal of Geophysical Research: Space Physics*, *124*(2),

546   1063-1084. doi: 10.1029/2018JA026183

547 Watt, C. E. J., Allison, H. J., Thompson, R. L., Bentley, S. N., Meredith, N. P.,

548   Glauert, S. A., . . . Rae, I. J. (2021). The Implications of Temporal Variability

549   in Wave-Particle Interactions in Earth's Radiation Belts. *Geophysical Research*

550   *Letters*, *48*(1). doi: 10.1029/2020GL089962